# Self-Powered Ultra-broadband Photodetector Monolithically Integrated on a PMN-PT Ferroelectric Single Crystal

*Huajing Fang,*[a] *Chao Xu,*[a] *Jie Ding,*[a] *Qiang Li,*[a] *Jia-Lin Sun,*[b] *Ji-Yan Dai,*[c] *Tian-Ling Ren,*[d] *and Qingfeng Yan*,*[a]

[a] Department of Chemistry, Tsinghua University, Beijing, 100084, China

[b] Collaborative Innovation Center of Quantum Matter, State Key Laboratory of Low-Dimensional Quantum Physics, Department of Physics, Tsinghua University, Beijing, 100084, China.

[c] Department of Applied Physics, The Hong Kong Polytechnic University, Hong Kong, China.

[d] Institute of Microelectronics, Tsinghua University, Beijing, 100084, China .

**KEYWORDS:** ultra-broadband, photodetector, self-powered, ferroelectric, pyroelectric.

**ABSTRACT:** Photodetectors capable of detecting two or more bands simultaneously with a single system have attracted extensive attentions because of their critical applications in image sensing, communication and so on. Here, we demonstrate a self-powered ultra-broadband

photodetector monolithically integrated on a $0.72Pb(Mg_{1/3}Nb_{2/3})O_3$-$0.28PbTiO_3$ (PMN-28PT) single crystal. By combining the optothermal and pyroelectric effect, the multifunctional PMN-28PT single crystal can response to a wide wavelength range from UV to terahertz (THz). At room temperature, the photodetector could generate a pyroelectric current under the intermittent illumination of incident light in absence of external bias. A systematic study of the photoresponse was investigated. The pyroelectric current shows an almost linear relationship to illumination intensity. Benefit from the excellent pyroelectric property of PMN-28PT single crystal and the optimized device architecture, the device exhibited a dramatic improvement in operation frequency up to 3 kHz without any obvious degradation in sensitivity. Such a self-powered photodetector with ultra-broadband response may open a window for the novel application of ferroelectric materials in optoelectronics.

## ■ INTRODUCTION

Photodetectors that convert light into an electrical signal are of paramount significance in a wide range of applications, such as environmental monitoring, imaging techniques, and optical communications.[1-5] In the past few years, the capability to detect light over a broad spectral range with a single system has drawn much attention in detectors, especially for those applications where high integration is required, such as space technology.[6-8] The commonly used strategy is searching suitable semiconductors with broadband absorption. Several recent attempts have been made in both organic and inorganic active materials.[9-13] However, the goal of ultra-broadband response from UV to THz is very difficult to be achieved in a single material with a simple structure. Furthermore, an external electric field was usually applied as the driving force to separate the photogenerated e-h pairs in all the above mentioned photodetectors. The external

power sources not only consumed energy but also largely increased the system size and cost.[14] Hence, making the photodetectors operate independently, sustainably and wirelessly is one of the most critical issues to further expand their scope of applications.[15]

Self-powered photodetecting based on the pyroelectric effect is an essential solution to overcome these problems, which has attracted a great deal of interest. Unlike the semiconductors which can only respond to incident photons with energy higher than their band gap, pyroelectric photodetectors based on the temperature induced spontaneous polarization change exhibited wavelength independent response.[16-18] However, traditional pyroelectric photodetectors suffered from weak photoresponse and relatively low response speed.[19,20] To improve the device performance, pyroelectric materials with high figures of merits (FOMs) are urgent needed. The (1-*x*)$Pb(Mg_{1/3}Nb_{2/3})O_3$-*x*$PbTiO_3$ (PMN-*x*PT) single crystal grown by the modified Bridgman technique has been reported to be a promising candidate. [111]-oriented rhombohedral PMN-PT single crystals exhibit excellent pyroelectric FOM, better than the traditional pyroelectric materials such as triglycine sulfate (TGS) and $LiTaO_3$.[21-23] Easy machining, chemical inert and uncooled operation further increase the competitive advantage of PMN-PT single crystals in practical applications.[24-26] As for response speed, optimizing device structure to improve the heat transfer should be an effective approach to realize fast response. To the best of our knowledge, there has no related report on PMN-PT single crystals regarding their application in ultra-broadband photodetector until now.

In this work, we demonstrate the first self-powered ultra-broadband photodetector monolithically integrated on a ferroelectric 0.72$Pb(Mg_{1/3}Nb_{2/3})O_3$-0.28$PbTiO_3$ (PMN-28PT) single crystal. The light of different wavelengths were detected with the same material due to the pyroelectric current accompanied by temperature oscillation. Thanks to the unique material

property and proper structure design, the device shows a fast operation frequency more than 3 kHz without any obvious degradation in sensitivity. The incident light in a wide wavelength range from UV to terahertz can be detected with zero bias. Hence, the ultra-broadband photodetector could operate independently and sustainably. Our results highlight a promising route for the novel application of ferroelectric materials in optoelectronics.

## ■ EXPERIMENTAL SECTION

The [111]-oriented PMN-28PT specimen ($5 \times 5 \times 0.5$ mm$^3$) was cut from a single crystal grown by the modified Bridgman method.[27] The specimen was thinned to 100 μm thick using a mechanical method and followed by finely polishing. Au electrode was deposited onto the bottom surface of the polished sample by ion beam sputtering. While the transparent electrode was obtained by drop-casting silver nanowires (Ag NWs, Nanjing XFNANO Materials Tech Co., Ltd) on the top surface. Before drop-casting, the Ag NWs ink was firstly diluted in ethanol and sonicated for 15 min. Then, the sample was poled for 30 min under an applied electric field of 2 kV/mm in the designed direction at room temperature.

SEM image of Ag NWs electrode was taken on the field-emission scanning electron microscopy (FESEM, JEOL JSM-6335F). The transmittance of Ag NWs electrode and the absorption spectrum of PMN-28PT single crystal plate were recorded by a Lambda 950 UV-Vis-NIR spectrophotometer (PerkinElmer). The lattice structure of [111]-oriented PMN-28PT single crystal was characterized through X-ray diffraction (XRD, Bruker D8-Advance) using Cu Kα radiation. The P-E loop and temperature dependent polarization of PMN-28PT single crystal were measured with a TF2000 Analyzer (aixACCT Systems). The domain structures were observed by a polarized light microscope (XJZ-6) along the [111] direction. A precision source/measure unit (Agilent B2911A) was used to assess the performance of the photodetector

under the illumination of UV (375 nm wavelength) to IR (10.6 μm wavelength) light with different wavelengths. The THz irradiation was generated by a 2.52 THz gas laser (FIRL 100, Edinburgh Instruments Ltd.).

## ■ RESULTS AND DISCUSSION

Figure 1(a) shows a schematic of the produced ultra-broadband photodetector with a simple parallel-plate capacitor structure. The [111]-oriented PMN-28PT ferroelectric single crystal was the core part of the device. (Some details about this material can be found in Figure S1, Supporting Information.) The composition of this crystal was located in the rhombohedral phase so that an almost single domain configuration could be obtained after poling along [111] direction. It was sandwiched between the bottom Au electrode and the top Ag NWs electrode. Considering the effective absorbance of incident light by PMN-28PT, at least one of the electrodes has to be transparent. Here, Ag NWs electrode was applied due to the perfect combination of transparency and electrical conductivity. Figure 1(b) shows a photograph of the Ag NWs electrode coated on a quartz substrate, in which the logo on the card behind the quartz substrate is clearly visible. Figure 1(c) plots the spectral transmittance of the as-prepared Ag NWs electrode. It exhibits a high transmittance over a broad wavelength ranging from 200 to 2300 nm which covers the region from UV to IR. As revealed by the inset SEM image, the random distribution of Ag NWs can form a conductive networks with the sheet resistance of ~30 Ω/□. Such a good conductivity is conducive to the collection of charge carriers.

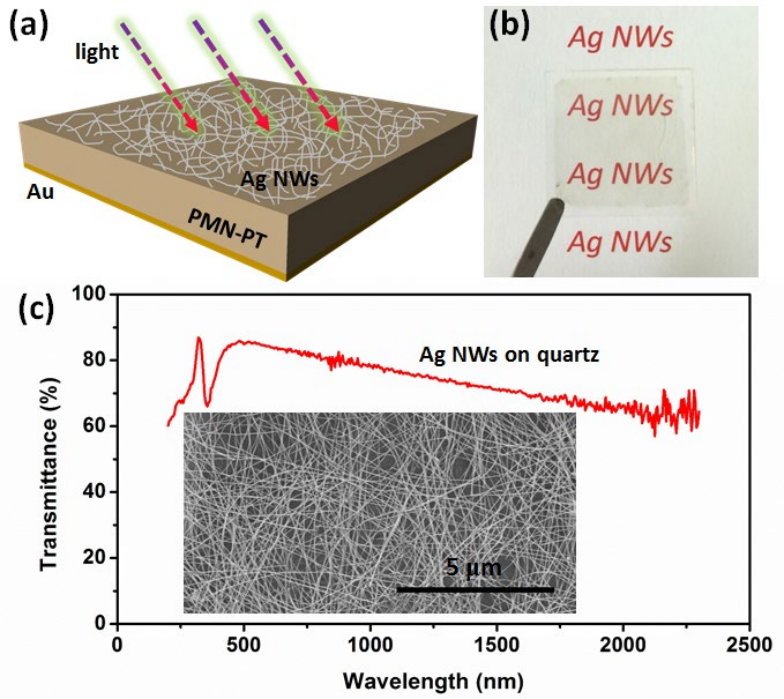


**Figure 1.** (a) A schematic diagram of the ultra-broadband photodetector. (b) A photograph of the quartz substrate coated with Ag NWs. (c) Optical transmittance from UV to near IR region of the as-prepared Ag NWs electrode. Inset is the SEM image of the Ag NWs electrode.

PMN-PT single crystals are known especially due to their excellent piezoelectric property which makes them extremely useful in the applications of electromechanical conversion such as ultrasonic transducers and hydrophones.[27-29] At the same time, the multifunctional PMN-PT single crystal can also handle photodetecting. But the detecting is based on another physical principle, namely, pyroelectric effect. Considering the anisotropy of pyroelectric coefficient ($p$) in single crystals, the [111]-oriented specimen was selected in our design for the maximization of $p$ component perpendicular to the electrodes. Figure 2(a) shows the XRD pattern of the polished PMN-28PT specimen. The only sharp diffraction peak assigned to (111) plane implies the precise orientation. The temperature dependence of polarization ($P_s$) from 20 to 180 ºC was recorded in Figure 2(b), thus the pyroelectric coefficient can be calculated by,

$$p = dP_s / dT \qquad (1)$$

A high $p$ value of $7.5 \times 10^{-4}$ C/m$^2$·K was found at room temperature, suggesting the potential of pyroelectric detecting. Such a high pyroelectric coefficient can also be regarded as the result of domain engineering. Since the direction of spontaneous polarization in rhombohedral PMN-28PT crystal is along [111] direction, the "1R" domain configuration can be obtained after poling along [111] direction. As shown in the inset in Figure 2(b), the external electric field during poling destroyed the symmetry of eight equivalent direction to form a single domain configuration, which is a preference of pyroelectric property. Polarizing light microscopy (PLM) observation of domain structure and extinction angle can give an intuitive evidence to confirm this "1R" domain configuration. As shown in Figure 2(c), the domain structure in visual region shows the extinction of all angles between 0 to 90°. The absence of birefringence indicates that the optical axis (*i.e.* the direction of spontaneous polarization) in each part of the specimen is along the thickness direction.

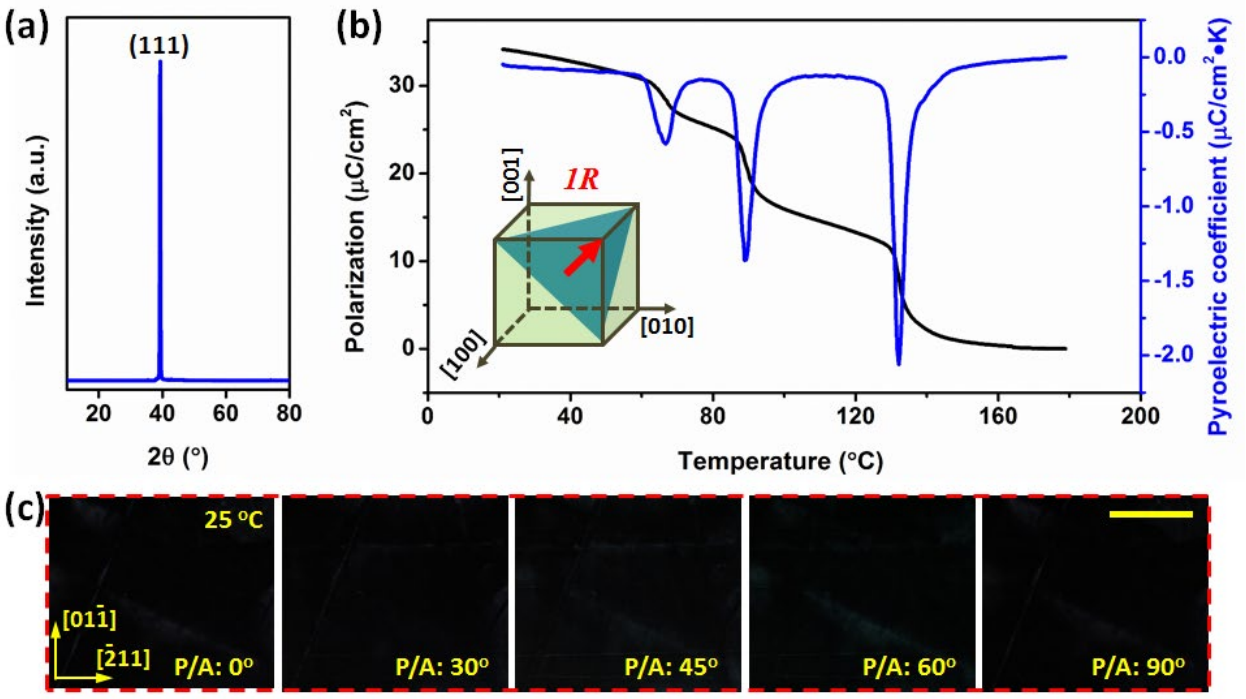

**Figure 2.** (a) The XRD pattern of the as-prepared [111]-oriented PMN-28PT single crystal. (b) The polarization and pyroelectric coefficient as a function of temperature for the [111]-oriented PMN-28PT single crystal. Inset is a schematic illustration of "1R" domain configuration of [111]-poled rhombohedral crystal. (c) Domain structures of a $[111]_c$ platelet observed by PLM after poling. The scale bar is 200 μm.

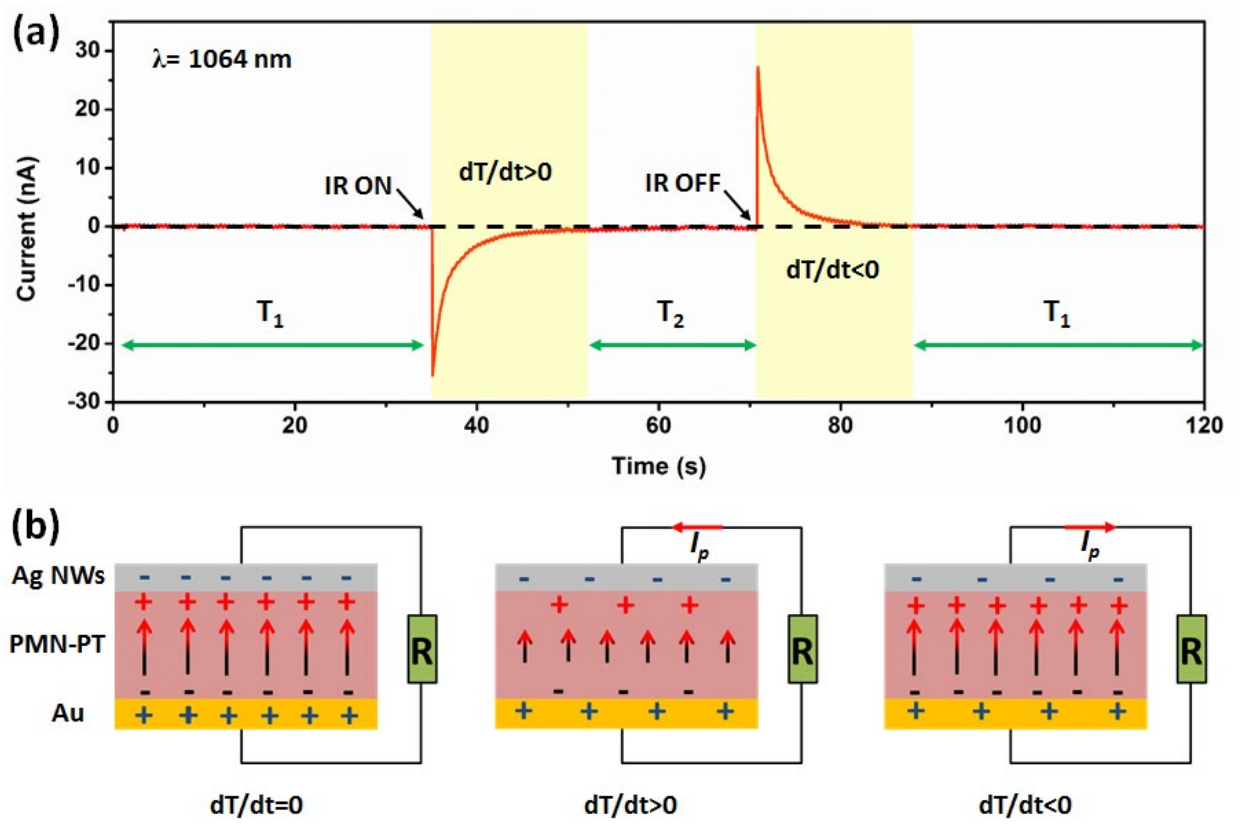


**Figure 3.** (a) The pyroelectric current measured from the poled [111]-oriented PMN-28PT single crystal under an intermittent illumination of 1064 nm IR light. (b) The schematic illustration of the temperature oscillation caused pyroelectric current.

Next, we characterized the photoresponse switching behavior to study the working principle of the device. Figure 3(a) shows the pyroelectric current generated by the photodetector under the intermittent illumination of 1064 nm IR light. At the initial state (room temperature $T_1$), the arrangement of dipoles after poling caused the bound charges on the surface of PMN-28PT single crystal. These bound charges were shielded by an equal amount of free charges. Thus, there was no output current at a fixed temperature, as shown in Figure 3(b). When the device was exposed to IR light, the PMN-28PT crystal was heated to a higher temperature. The bound

charge is reduced since the level of polarization decreases on heating. In order to maintain the static balance, excess free charges discharged across the external load. This process resulted in a negative current signal under the short circuit condition. The magnitude of the current gradually decreased to zero when a new thermal equilibrium state at the temperature of $T_2$ (high than $T_1$) was achieved. Similarly, shading the device from IR illumination caused a cooling effect under natural convection, hence a positive current signal was observed. The pyroelectric current ($I_{pyro}$) in both cases is given by,

$$I_{pyro} = pAdT / dt \qquad (2)$$

Here, $A$ is the surface area of the sample and $dT/dt$ is the first derivative of temperature with respect to time. Figure 4(a) plots the relationship between pyroelectric current and the illumination intensity. The corresponding responsivity ($R$) was also calculated as the ratio of pyroelectric current divided by the IR intensity. The value of the pyroelectric current almost linearly increased with the IR intensity, because the higher IR intensity caused a relatively larger $dT/dt$ under the same chopping frequency. The responsivity also shows a positive correlation with the intensity, the highest responsivity was 88.5 nA/W at an intensity of 3.5 W/cm$^2$. The relationship between the output voltage signals and illumination intensity can be found in Figure S2, Supporting Information.

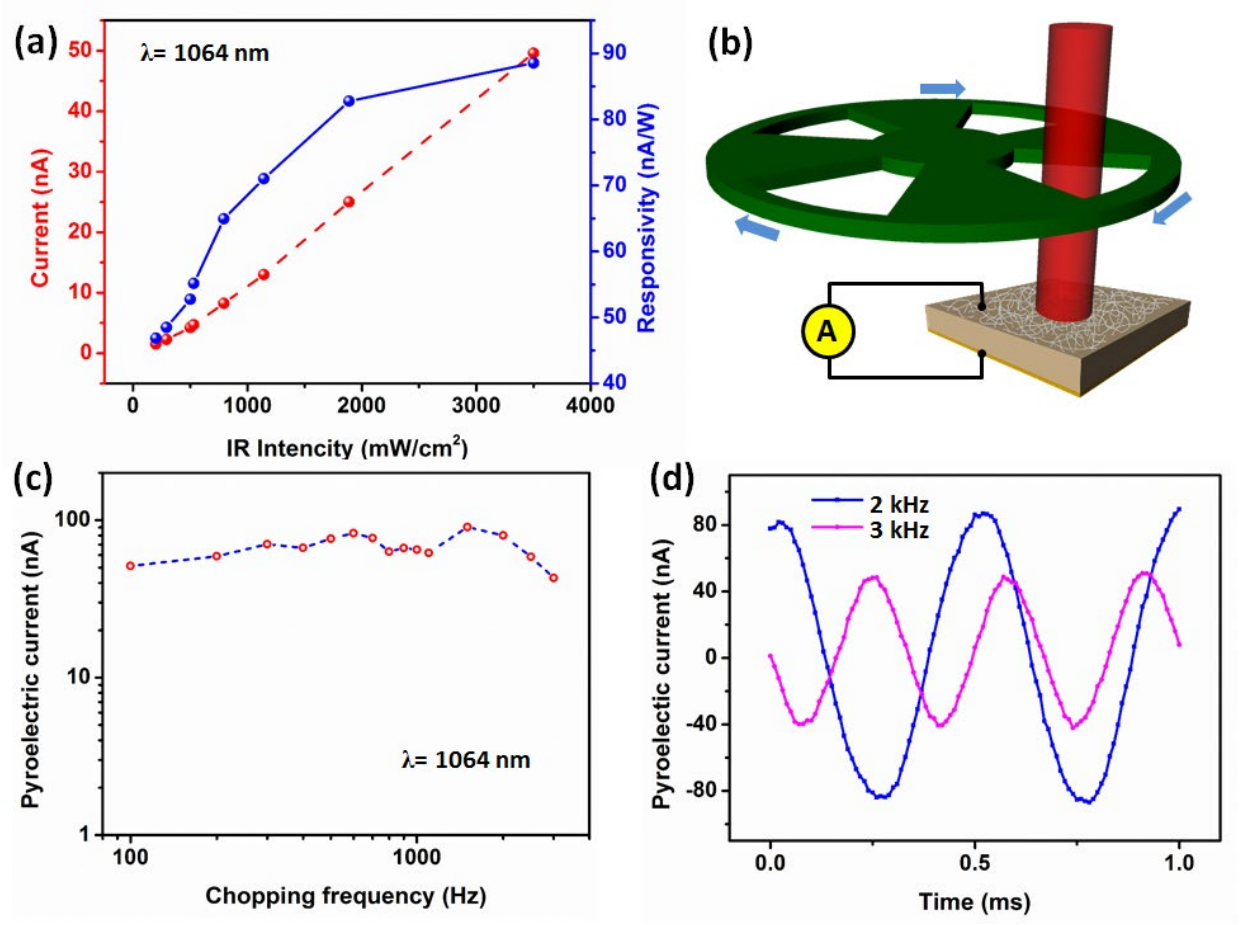


**Figure 4.** (a) The measured pyroelectric current and the current responsivity of the photodetector under the on-off switching of 1064 nm IR with different illumination intensities. (b)The schematic measurement system for fast IR detecting with tunable chopping frequency. (c) Pyroelectric current as a function of chopping frequency for 1064 nm IR with an intensity of 3.5 W/cm$^2$. (d) The pyroelectric response of the self-powered photodetector when chopped at 2 and 3 kHz.

For motion detection and dynamic imaging, the frequency response of the IR detector is also a very important property. Unfortunately, traditional pyroelectric detectors generally have a poor frequency response around 100 Hz due to their operation principles.[30] Firstly, the incident IR radiation is absorbed by the top electrode and converts into heat. Then the heat needs to conduct to the pyroelectric layer and changes its temperature. Finally, the temperature oscillation stimulates the polarization variation for detection. The relaxation time of the spontaneous polarization in crystals is as short as $10^{-12}$ s,[31] hence the poor frequency response is mainly

caused by the delay between radiation absorption and temperature oscillation. Replacing the fully covered electrode with a partially covered electrode has been proved an effective solution to improve the thermal diffusion.[32] In this work, a fast frequency response has been achieved by a clever exploiting of the Ag NWs transparent electrode. Distinct from the traditional way, the entire PMN-28PT crystal was heated by directly absorbing the IR radiation rather than heat conduction from the top electrode. The implementation of Ag NWs not only solved the delay of thermal diffusion but also avoided the heat losses during heat conduction. Figure 4(b) shows the measurement system for fast IR detecting. The pulsed incident light was generated by modulating the 1064 nm laser with a mechanical chopper. Figure 4(c) plots the pyroelectric current measured at zero bias voltage under different chopping frequency. There has no significant decrease in order of magnitude even chopped at 3 kHz. The detailed output signals at 2 and 3 kHz can be found in Figure 4(d). Such a dramatic improvement in operation frequency would break the limit of pyroelectric detector in high-speed response applications such as motion detection and dynamic imaging.

In addition to the improvement of operation frequency, the photodetector also exhibits the advantage of ultra-broadband sensitivity. Figure 5(a) plots the spectral response of the self-powered photodetector measured in a wide wavelength range from 375 nm to 118.8 μm. In all the case, pyroelectric current signals were generated by combining with the optothermal conversion. The lattice vibration of PMN-28PT crystal can be intensified after absorbing the incident photons. Unlike the optoelectronic conversion in semiconductors, the optothermal conversion shows no selectivity in wavelengths. Theoretically, there is no wavelength limit for our device. Figure 5(b) presents the photoswitching curves of the photodetector during repetitive illumination of four representative wavelengths. Although the incident intensity of each light is

kept around 100 mW, the pyroelectric current at short wavelengths are much higher. We believe that the enhanced optothermal energy conversion at short wavelengths benefits from the excitation of surface plasmons in the top Ag NWs electrode. As reported in the previous works,[33-36] light-matter interactions can be enhanced by introducing plasmonic nanostructures based on noble metals. Here, the excellent plasmonic properties of Ag NWs at short wavelengths might lead to a stronger light absorption and further intensify the lattice vibration of PMN-28PT crystal. It should be mentioned, ferroelectric photovoltaic effect[37-39] may also exist in our device. But we have proved that it was not the main mechanism of photoresponse. The details are provided in Figure S3, Supporting Information.

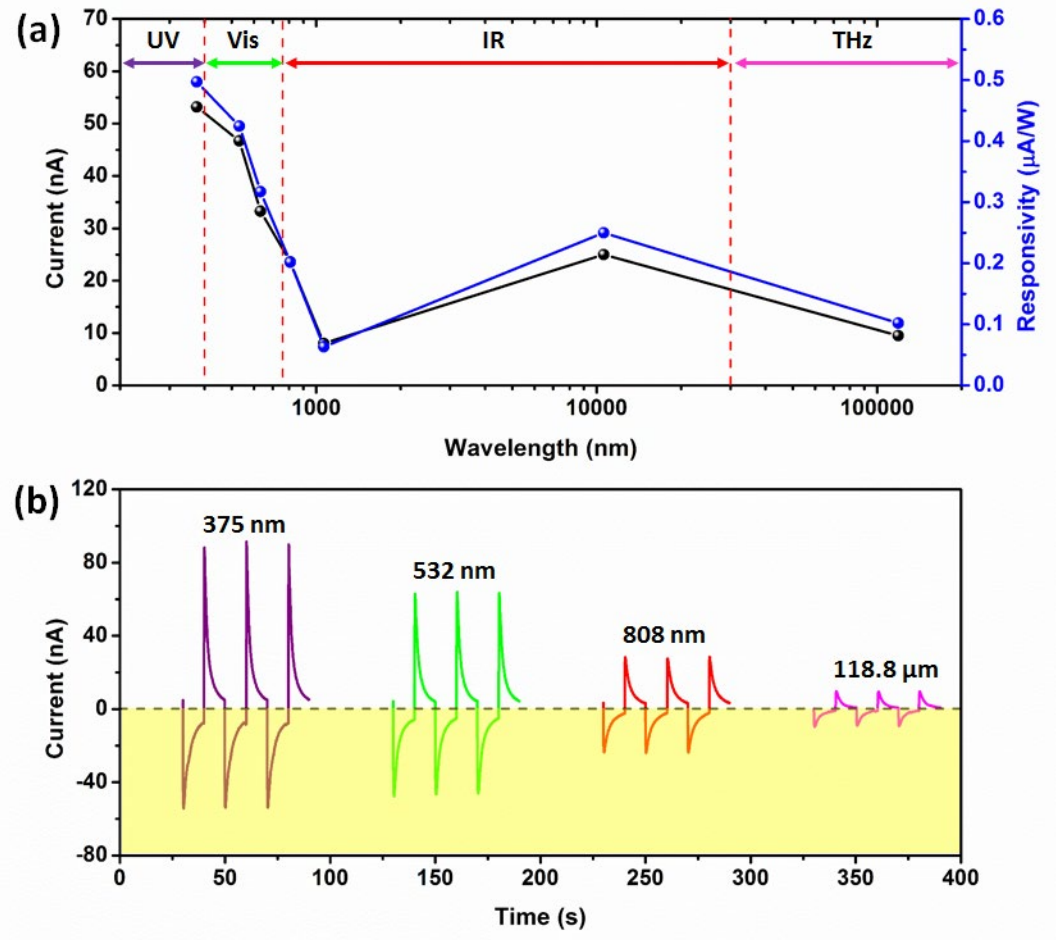


**Figure 5.** (a) The spectral response of the self-powered photodetector measured in a wide wavelength range from 375 nm to 118.8 μm, the intensity of each light is about 100 mW. (b) The

typical photoswitching behavior under illuminations with wavelengths of 375 nm (UV), 532 nm (Vis), 808 nm (IR) and 118.8 μm (THz).

## ■ CONCLUSION

In summary, we have demonstrated a self-powered photodetector monolithically integrated on a PMN-28PT single crystal which has an ultra-broadband response for the first time. The working principle is based on the combination of optothermal effect and pyroelectric effect in PMN-28PT single crystal. The photodetector can exhibit a responsivity of ~90 nA/W at 1064 nm without any external power supply. Meanwhile, the device also shows a fast pyroelectric response by implementation of Ag NWs as a top electrode. A dramatic improvement in operation frequency up to 3 kHz without any obvious degradation in sensitivity was achieved. The device based on a PMN-28PT single crystal exhibits definite photoresponse to the light from UV to THz region. At short wavelengths, the pyroelectric signals can be further enhanced possibly by the excitation of surface plasmons in Ag NWs electrode. Such an ultra-broadband photodetector demonstrates a great potential for the application of ferroelectric materials in optoelectronics.

## ■ ASSOCIATED CONTENT

### Supporting Information

The Supporting Information is available free of charge on the ACS Publications website at DOI: Some details about the PMN-28PT material, the relationship between the output voltage signals and illumination intensity, the discussion of ferroelectric photovoltaic. (PDF)

## ■ AUTHOR INFORMATION

### Corresponding Author

*E-mail: *yanqf@mail.tsinghua.edu.cn*.

**Notes**

The authors declare no competing financial interest.

## ■ ACKNOWLEDGMENT

This research was supported by the National key Basic Research Program of China (973 Program) under Grant No. 2013CB632900 and the National Science Foundation of China (No. 91333109). The Tsinghua University Initiative Scientific Research Program (Nos. 20131089202 and 20161080165) and the Open Research Fund Program of the State Key Laboratory of Low-Dimensional Quantum Physics (No. KF201516) are also acknowledged for partial financial support. Dr. Yingxin Wang from Key Laboratory of Particle and Radiation Imaging, Ministry of Education and Department of Engineering Physics, Tsinghua University is acknowledged for THz spectrum measurement.

## ■ REFERENCES

(1) Hu, L. F.; Brewster, M. M.; Xu, X. J.; Tang, C. C.; Gradečak, S.; Fang, X. S. Heteroepitaxial Growth of GaP/ZnS Nanocable with Superior Optoelectronic Response. *Nano Lett.* **2013**, *13*, 1941-1947.

(2) Zhai, T. Y.; Li, L.; Wang, X.; Fang, X. S.; Bando, Y.; Golberg, D. Recent Developments in One-Dimensional Inorganic Nanostructures for Photodetectors. *Adv. Funct. Mater.* **2010**, *20*, 4233-4248.

(3) Wang, Z. N.; Yu, R. M.; Wen, X. N.; Liu, Y.; Pan, C. F.; Wu, W. Z.; Wang, Z. L. Optimizing Performance of Silicon-Based p-n Junction Photodetectors by the Piezo-Phototronic Effect. *ACS Nano* **2014**, *8*, 12866-12873.

(4) Lee, S. Y.; Park, K. I.; Huh, C.; Koo, M.; Yoo, H. G.; Kim, S.; Ah, C. S.; Sung, G. Y.; Lee, K. J. Water-Resistant Flexible GaN LED on a Liquid Crystal Polymer Substrate for Implantable Biomedical Applications. *Nano Energy* **2012**, *1*, 145-151.

(5) Fang, X. S.; Wu L. M.; Hu, L. F. ZnS Nanostructure Arrays: A Developing Material Star. *Adv. Mater.* **2011**, *23*, 585-598.

(6) Cao, Y.; Zhu, J. Y.; Xu, J.; He, J. H.; Sun, J.-L.; Wang, Y. X.; Zhao Z. R. Ultra-Broadband Photodetector for the Visible to Terahertz Range by Self-Assembling Reduced Graphene Oxide-Silicon Nanowire Array Heterojunctions. *Small* **2014**, *10*, 2345-2351.

(7) Liu, C. H.; Chang, Y. C.; Norris, T. B.; Zhong, Z. H. Graphene Photodetectors with Ultra-broadband and High Responsivity at Room Temperature. *Nat. Nanotechnol.* **2014**, *9*, 273-278.

(8) Yoo, J.; Jeong, S.; Kim, S.; Je, J. H. A Stretchable Nanowire UV-Vis-NIR Photodetector with High Performance. *Adv. Mater.* **2015**, *27*, 1712-1717.

(9) Chen, S.; Teng, C. J.; Zhang, M.; Li, Y. R.; Xie, D.; Shi, G. Q. A Flexible UV-Vis-NIR Photodetector based on a Perovskite/Conjugated-Polymer Composite. *Adv. Mater.* **2016**, *28*, 5969-5974.

(10) Yang, X. G.; Liu, Y.; Lei, H. X.; Li, B. J. An organic-inorganic Broadband Photodetector based on a Single Polyaniline Nanowire Doped with Quantum Dots. *Nanoscale*, **2016**, *8*, 15529-15537.

(11) Gao, L.; Chen, C.; Zeng, K.; Ge, C.; Yang, D.; Song, H. S.; Tang, J. Broadband, Sensitive and Spectrally Distinctive $SnS_2$ Nanosheet/PbS Colloidal Quantum Dot Hybrid Photodetector. *Light: Sci. Appl.* **2016**, *5*, e16126.

(12) Buscema, M.; Groenendijk, D. J.; Blanter, S. I.; Steele, G. A.; Zant, H. S. J.; Castellanos-Gomez, A. Fast and Broadband Photoresponse of Few-Layer Black Phosphorus Field-Effect Transistors. Nano Lett. 2014, 14, 3347-3352.

(13) Zhang, Y.; Liu, T.; Meng, B.; Li, X. H.; Liang, G. Z.; Hu, X. N.; Wang, Q. J. Broadband High Photoresponse from Pure Monolayer Graphene Photodetector. *Nat. Commun.* **2013**, *4*, 1811.

(14) Peng, L.; Hu, L. F.; Fang, X. S. Energy Harvesting for Nanostructured Self-Powered Photodetectors. *Adv. Funct. Mater.* **2014**, *24*, 2591-2610.

(15) Fang, H. J.; Li, Q.; Ding, J.; Li, N.; Tian, H.; Zhang, L. J.; Ren, T. L.; Dai, J. Y.; Wang, L. D.; Yan, Q. F. Self-Powered Organolead Halide Perovskite Single Crystal Photodetector Driven by a DVD-Based Triboelectric Nanogenerator. *J. Mater. Chem. C* **2016**, *4*, 630-636.

(16) Sun, Z. H.; Tang, Y. Y.; Zhang, S. Q.; Ji, C. M.; Chen, T. L.; Hong, M. C.; Luo, J. H. Ultrahigh Pyroelectric Figures of Merit Associated with Distinct Bistable Dielectric Phase

Transition in a New Molecular Compound: Di-n-Butylaminium Trifluoroacetate. *Adv. Mater.* **2015**, *27*, 4795-4801.

(17) Botea, M.; Iuga, A.; Pintilie, L. Giant Pyroelectric Coefficient Determined from the Frequency Dependence of the Pyroelectric Signal Generated by Epitaxial $Pb(Zr_{0.2}Ti_{0.8})O_3$ Layers Grown on Single Crystal $SrTiO_3$ Substrates. *Appl. Phys. Lett.* **2013**, *103*, 232902.

(18) Kesim, M. T.; Zhang, J.; Trolier-McKinstry, S.; Mantese, J. V.; Whatmore, R. W.; Alpay, S. P. Pyroelectric Response of Lead Zirconate Titanate Thin Films on Silicon: Effect of Thermal Stresses. *J. Appl. Phys.* **2013**, *114*, 204101.

(19) Wu, C. G.; Li, P.; Cai, G. Q.; Luo, W. B.; Sun, X. Y.; Peng, Q. X.; Zhang, W. L. Quick Response PZT/P(VDF-TrFE) Composite Film Pyroelectric Infrared Sensor with Patterned Polyimide Thermal Isolation Layer. *Infrared Phys. Technol.* **2014**, *66*, 34-38.

(20) Akai, D.; Hirabayashi, K.; Yokawa, M.; Sawada, K.; Taniguchi, Y.; Murashige, S.; Nakayamac, N.; Yamada, T,; Murakami, K.; Ishida, M. Pyroelectric Infrared Sensors with Fast Response Time and High sensitivity Using Epitaxial $Pb(Zr,Ti)O_3$ Films on Epitaxial $\gamma$-$Al_2O_3$/Si Substrates. *Sens. Actuators, A* 2006, 130, 111-115.

(21) Li, L.; Zhao, X. Y.; Li, X. B.; Ren, B.; Xu, Q.; Liang, Z.; Di, W. N.; Yang, L. R.; Luo, H. S.; Shao, X. M.; Fang, J. X.; Neumann, N.; Jiao, J. Scale Effects of Low-Dimensional Relaxor Ferroelectric Single Crystals and Their Application in Novel Pyroelectric Infrared Detectors. *Adv. Mater.* **2014**, *26*, 2580-2585.

(22) Tang, Y. X.; Zhao, X. Y.; Feng, X. Q.; Jin, W. Q.; Luo, H. S. Pyroelectric Properties of [111]-oriented $Pb(Mg_{1/3}Nb_{2/3})O_3$-$PbTiO_3$ Crystals. *Appl. Phys. Lett.* **2005***, 86*, 082901.

(23) Feng, Z. Y.; Zhao, X. Y.; Luo, H. S. Large Pyroelectric Effect in Relaxor-Based Ferroelectric $Pb(Mg_{1/3}Nb_{2/3})O_3$-$PbTiO_3$ Single Crystals. *J. Am. Ceram. Soc.* **2006**, *89*, 3437-3440.

(24) Ko, Y. J.; Park, Y. K.; Yun, B. K.; Lee, M.; Jung, J. H. High Pyroelectric Power Generation of $0.7Pb(Mg_{1/3}Nb_{2/3})$ $O_3$-$0.3PbTiO_3$ Single Crystal. *Curr. Appl. Phys.* **2014**, 14, 1486-1491.

(25) Zhao, X.; Wu, X.; Liu, L.; Luo, H. S.; Neumann, N.; Yu, P. Pyroelectric Performances of Relaxor-based Ferroelectric Single Crystals and Related Infrared Detectors. *Phys. Status Solidi A* **2011**, *208*, 1061-1067.

(26) Fang, H. J.; Lin, Z. Y.; Wang, X. S.; Tang, C. Y.; Chen, Y.; Zhang, F.; Chai, Y.; Li, Q.; Yan, Q. F.; Chan, H. L. W.; Dai, J. Y. Infrared Light Gated $MoS_2$ Field Effect Transistor. *Opt. Express* **2015**, *23*, 31908-31914.

(27) Zhang, S. J.; Li, F. High Performance Ferroelectric Relaxor-$PbTiO_3$ Single Crystals: Status and Perspective. *J. Appl. Phys.* **2012**, *111*, 031301.

(28) Sun E. W.; Cao, W. W. Relaxor-Based Ferroelectric Single Crystals: Growth Domain Engineering, Characterization and Application. *Prog. Mater. Sci.* **2014**, *65*, 124-210.

(29) Lee, H. J.; Zhang, S. J.; Luo, J.; Li, F.; Shrout, T. R. Thickness-Dependent Properties of Relaxor-$PbTiO_3$ Ferroelectrics for Ultrasonic Transducers. *Adv. Funct. Mater.* **2010**, *20*, 3154-3162.

(30) Kulkarni, E. S.; Heussler, S. P.; Stier, A. V.; Martin-Fernandez, I.; Andersen, H.; Toh, C. T.; Özyilmaz, B. Exploiting the IR Transparency of Graphene for Fast Pyroelectric Infrared Detection. *Adv. Optical Mater.* **2015**, *3*, 34-38.

(31) Auston D. H.; Glass, A. M. Optical Generation of Intense Picosecond Electrical Pulses. *Appl. Phys. Lett.* **1972**, *20*, 398-399.

(32) Zabek, D.; Taylor, J.; Boulbar, E. L.; Bowen, C. R. Micropatterning of Flexible and Free Standing Polyvinylidene Difluoride (PVDF) Films for Enhanced Pyroelectric Energy Transformation. *Adv. Energy Mater.* **2015**, *5*, 1401891.

(33) Lee, Y. C.; Lin, K. T.; Chen, H. L. Ultra-broadband and Omnidirectional Enhanced Absorption of Graphene in a Simple Nanocavity Structure. *Carbon* **2016**, *108*, 253-261.

(34) Kang, M. G.; Xu, T.; Park, H. J.; Luo, X.; Guo, L. J. Efficiency Enhancement of Organic Solar Cells Using Transparent Plasmonic Ag Nanowire Electrodes. *Adv. Mater.* **2010**, *22*, 4378-4383.

(35) Groep, J.; Spinelli, P.; Polman, A. Transparent Conducting Silver Nanowire Networks, *Nano Lett.* **2012**, *12*, 3138-3144.

(36) Liu, Y.; Cheng, R.; Liao, L.; Zhou, H. L.; Bai, J. W.; Liu, G.; Liu, L.; Huang, Y.; Duan, X. F. Plasmon Resonance Enhanced Multicolour Photodetection by Graphene, *Nat. Commun.* **2011**, *2*, 579.

(37) Yang, S. Y.; Seidel, J.; Byrnes, S. J.; Shafer, P.; Yang, C.-H.; Rossell, M. D.; Yu, P.; Chu, Y.-H.; Scott, J. F.; Ager III, J. W.; Martin, L. W.; Ramesh, R. Above-Bandgap Voltages from Ferroelectric Photovoltaic Devices. *Nat. Nanotechnol.* **2010**, *5*, 143-147.

(38) Dong, W.; Guo, Y. P.; Guo, B.; Li, H.; Liu, H. Z.; Joel, T. W. Enhanced Photovoltaic Effect in $BiVO_4$ Semiconductor by Incorporation with an Ultrathin $BiFeO_3$ Ferroelectric Layer. *ACS Appl. Mater. Interfaces* **2013**, *5*, 6925-6929.

(39) Yi, H. T.; Choi, T.; Choi, S. G.; Oh, Y. S.; Cheong, S.-W. Mechanism of the Switchable Photovoltaic Effect in Ferroelectric $BiFeO_3$. *Adv. Mater.* **2011**, *23*, 3403-3407.

Table of Contents Graphic